JOURNAL OF SOLID STATE CHEMISTRY 113, 296–302 (1994)

The Structure of Na_3SbTe_3: How Ionic and Covalent Bonding Forces Work Together

Jianhua Lin and Gordon J. Miller[1]

Department of Chemistry, Iowa State University, Ames, Iowa 50011

Received January 19, 1994; in revised form February 25, 1994; accepted March 3, 1994

The compound Na_3SbTe_3 has been synthesized from the elements and characterized by single crystal X-ray diffraction. Na_3SbTe_3 is cubic, crystallizing in the $cP28$ structure type (isomorphous with Na_3AsS_3); space group $P2_13$ (No. 198); $a = 9.6114(9)$ Å; $Z = 4$; $R1 = 0.0324$; $wR2 = 0.0561$ ($I \geq 2\sigma(I)$). The structure consists of isolated sodium cations and trigonal pyramidal $[SbTe_3]^{-3}$ anions with a Sb–Te bond length of 2.787(1) Å and a Te–Sb–Te bond angle of 100.0(1)°. The structure is related to both the Li_3Bi and K_3AsS_4-type structures. Both lattice energy and semiempirical electronic structure calculations are utilized to evaluate various local and long-range structural aspects of this Zintl phase.

Ternary alkali metal pnictide–chalcogenides have been investigated extensively in the past 20 years (1, 2, and references therein). Among them, the structural details of alkali metal pnictide–sulfides as well as some of the pnictide–selenides are now well established, but there are only a few examples known for the pnictide–tellurides (3–10). In transition metal compounds, tellurides often exhibit different structural characteristics from sulfide and selenide analogs (11, 12). For this reason, we are interested in extending the structural chemistry of ternary pnictide–tellurides to probe their differences and similarities to the corresponding sulfides and selenides.

Ternary pnictide–chalcogenides often adopt structures that follow the Zintl–Klemm–Busmann scheme (13), which accounts for the connectivity among the electronegative main group atoms by using a modified 8-N rule to assign valence electrons. In these compounds, the environment of the pnicogen element is usually either three or four-bonded to chalcogen, i.e., "Pn^0" or "Pn^{1+}" using the Zintl–Klemm–Busmann concept. On the other hand, formal charges evaluated from an ionic viewpoint adopt values of either Pn^{3+}, with a lone pair of electrons, or Pn^{5+}. Due to small electronegativity differences between elements in these two columns of the periodic table (14), the true electronic distribution is probably at some point between these two extreme electron counting schemes. In particular, the classes of compounds A_3PnX_3 and A_3PnX_4 (A = alkali metal; Pn = pnicogen element; X = chalcogen element) provide a means of examining the stereochemical effect of a lone pair of electrons.

A large number of A_3PnS_3 (Pn = As, Sb) compounds have been reported, such as Na_3AsS_3, K_3AsS_3, Na_3SbS_3, and K_3SbS_3 (15). All of these compounds contain isolated alkali metal A^+ cations and $[PnS_3]^{-3}$ anions with a trigonal pyramidal geometry. Among these compounds, only Na_3AsS_3 has been characterized by single crystal X-ray diffraction, while the others were identified only by X-ray powder diffraction. The corresponding telluride phase Na_3SbTe_3 has been mentioned by Lazarev *et al.* (16) during an investigation of the phase diagram of the ternary Na–Sb–Te system, but they did not show any characterization of this compound, nor did they provide data from X-ray powder diffraction. Recently, Eisenmann and coworkers, as well as Jung *et al.*, have independently reported the single crystal structures of K_3SbTe_3 (3, 7) and K_3BiTe_3 (4). During attempts to synthesize new compounds based upon the three-dimensional network of $AgTe_3$ (17), we isolated the compound Na_3SbTe_3. In this paper, we report its crystal structure, which we have also characterized by a single crystal X-ray diffraction study, and examine both classical and quantum mechanical forces that influence its geometry.

EXPERIMENTAL

Synthesis. Na_3SbTe_3 is reported to be a stable solid phase below 703 K, but decomposes into Na_2Te and $NaSbTe_2$ above 703 K, before the onset of melting (16). Therefore, in order to grow single crystals suitable for single crystal X-ray diffraction, we employed excess antimony in the reaction. The reaction, which started from the elements in a Na : Sb : Te molar ratio of 1 : 2 : 1, was carried out in a sealed evacuated tantalum ampule at 1070 K for 24 hr, and subsequently cooled to room temperature after 24 hr. The product, which was identified by X-ray-

[1] To whom correspondence should be addressed.

0022-4596/94 $6.00

TABLE 1
Structure Determination Summary for Na_3SbTe_3

Space group	$P2_13$ (No. 198)
Unit cell dimenions	a = 9.6170(10) Å
Volume	889.4(2) Å^3
Z	4
Density (calc.)	4.283 Mg/m^3
Crystal size (mm)	0.15 × 0.10 × 0.10
Absorption coefficient	12.794 mm^{-1}
Radiation	Mo$K\alpha$ (λ = 0.71073 Å)
Temperature (K)	300(1)
2θ Range	2.0 to 50.0°
Scan range(ω)	0.70°
Scan speed	Variable; 5.00 to 30.00°/min in ω
Index ranges	$-1 \le h \le 13$, $-1 \le k \le 13$, $-13 < l \le 13$
Reflections collected	2199
Independent reflections	527 (R_{int} = 0.0862)
Observed reflections	443 ($I \ge 2\sigma(I)$)
Min./Max. transmission	0.596/0.974
Absolute structure	−0.34(16)
Extinction correction	0.0003(2)
Weighting scheme	$w = 1/[\sigma^2(F_0^2) + (0.0116P)^2]$ where $P = (F_0^2 + 2F_0^2)/3$
Parmaeters refined	23
Final R indices [$I \ge 2\sigma(I)$]	$R1$ = 0.0324, $wR2$ = 0.0561
R indices (all data)	$R1$ = 0.0460, $wR2$ = 0.0601
GooF, all data	1.042
observed data	1.013
Data-to-parameter ratio	28.4 : 1
Largest difference peak	0.721 e/Å^{-3}
Largest difference hole	−0.729 e/Å^{-3}

powder diffraction, was a mixture of gray-colored Na_3SbTe_3 and elemental antimony. They can be separated mechanically. Na_3SbTe_3 is moderately stable in air, and shows some decomposition over several hours as monitored by X-ray powder diffraction.

Structure determination. The X-ray powder diffraction pattern, taken with an Enraf–Nonius Guinier camera using monochromatized Cu$K\alpha_1$ radiation, with silicon powder as an internal standard, was successfully indexed with a cubic unit cell (a = 9.6114(9) Å) using 23 reflections in a 2θ range between 16° and 80°. Additional lines present on the powder pattern were identified and assigned to the rhombohedral structure of elemental antimony. Single crystals suitable for X-ray diffraction were selected in an argon-filled glove box and then sealed in glass capillaries. The cell parameters of a single crystal were determined by a least-squares analysis of 25 reflections with 20° ≤ 2θ ≤ 35° centered on a Siemens P4 diffractometer (a = 9.6170(10)). Further relevant crystallographic data are summarized in Table 1.

The systematic absences of the reflections $h00$, h = $2n$, indicate that both $P2_13$ and $P4_232$ are possible space groups. Upon checking the Laue symmetry as well as finding a possible isostructural compound in Na_3SbTe_3 (15), we selected space group $P2_13$. The structure was subsequently solved using direct methods (SHELXTL-PLUS (18)). The refinement utilized 443 reflections ($I \ge 2\sigma(I)$) for 23 parameters, and yielded the residuals R = 0.032, wR = 0.056, GooF = 1.04 (SHELXL-93 (19)). The difference Fourier map did not show any additional significant chemical features. Furthermore, comparison between the calculated and observed X-ray powder patterns showed excellent agreement of intensities, with the largest deviation of a 2θ value of 0.07°. Table 2 lists the positional and displacement parameters and Table 3 contains some selected bond lengths and bond angles for Na_3SbTe_3. Atomic scattering factors and anomalous dispersion corrections were taken from the *International Tables for X-Ray Crystallography* (20).

TABLE 2
Positional Coordinates and Equivalent Isotropic Displacement Coefficients for Na_3SbTe_3

Atom	Site	x	y	z	U_{eq}
Sb	4a	−0.0373(1)	−0.0373(1)	−0.0373(1)	0.021(1)
Te	12b	0.2378(1)	0.8813(1)	0.0030(1)	0.025(1)
Na(1)	4a	0.1842(7)	0.1842(7)	0.1842(7)	0.033(1)
Na(2)	4a	−0.3277(7)	−0.3277(7)	−0.3277(7)	0.030(1)
Na(3)	4a	0.4134(7)	0.4134(7)	0.4134(7)	0.048(2)

Note. All site occupation factors are 1.0.

Magnetic measurements. The magnetic susceptibility of Na_3SbTe_3 was measured using a Quantum Designs SQUID magnetometer operated at 2 T between 4 and 350 K. Na_3SbTe_3 shows temperature-independent diamagnetism, which is in accord with its closed shell electronic configuration.

DISCUSSION

Na_3SbTe_3 is isostructural with Na_3AsS_3 (15) and K_3SbTe_3 (3). As illustrated in Fig. 1, the structure contains isolated Na cations and trigonal pyramidal $[SbTe_3]^{-3}$ anions. The geometry of these $[SbTe_3]^{-3}$ anions (d(Sb–Te) = 2.787 Å; ∠Te–Sb–Te = 100.0°) strongly resembles the trigonal pyramidal anions in K_3SbTe_3(d(Sb–Te) = 2.783 Å; ∠Te–Sb–Te = 101.9°).

TABLE 3
Selected Bond Distances (Å) and Angles(°) in Na_3SbTe_3

Sb–Te	2.787(1), 3×	Te–Sb–Te	100.04(4), 3×
Na1–Te	3.224(5), 3×	Na1–Te	3.427(7), 3×
Na2–Te	3.216(5), 3×	Na2–Te	3.392(6), 3×
Na3–Te	3.308(6), 3×	Na3–Te	3.453(7), 3×

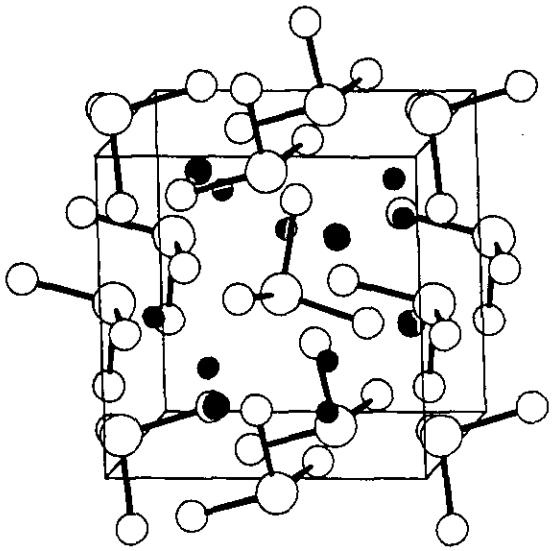

FIG. 1. (100) Perspective view of the unit cell of Na_3SbTe_3. Na, small dark circles; Sb, large open circles; Te, intermediate open circles.

Closer inspection of the coordination around each antimony atom, see Fig. 2a, reveals three additional Te atoms at a distance of 3.966(1) Å to form an extremely distorted Te coordination octahedron. This distortion from regular octahedral coordination is due to the presence of a lone pair of electrons at each Sb(3+) site. This lone pair, as predicted from either valence bond or molecular orbital theories, is directed along a threefold axis of the Na_3SbTe_3 structure. Andersson and co-workers (21, 22) have noted

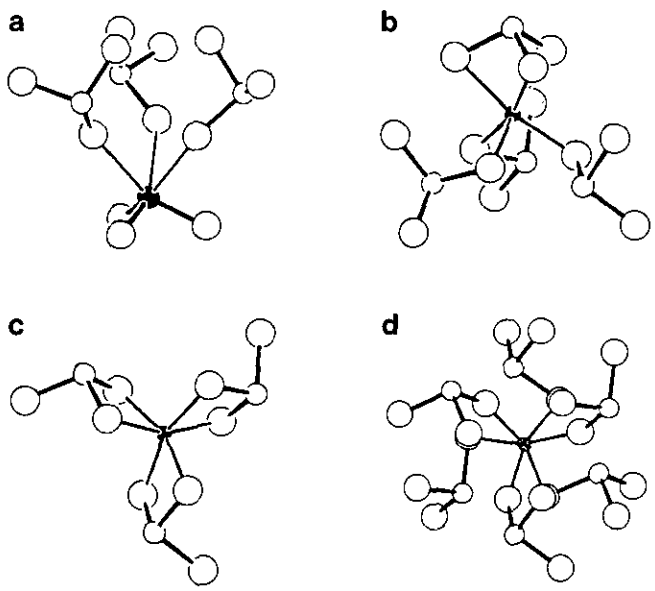

FIG. 2. Cation coordination in Na_3SbTe_3. (a) Sb, (b) Na1, (c) Na2, and (d) Na3. Dark circles indicate the coordinated cation.

that when the anions are larger than oxide or fluoride ions, the lone pair is often found at the center of the relatively large anion polyhedron. In Na_3SbTe_3, if we assume the "distance" between the Sb nucleus and the lone pair to be about 1.0 Å, as proposed by Galy *et al.* (21), the lone pair would be nearly at the center of the octahedron with the distance between the lone pair and coordinating Te atoms of ca. 3.3 Å. Similar coordination polyhedra have been observed in other Sb(III) compounds such as SbI_3 (23). Another effect of the lone pair is that the Te–Sb–Te bond angle (100.0°) within each $[SbTe_3]^{-3}$ unit is significantly smaller than the regular tetrahedral angle (109.5°) due to the repulsion between the lone pair and the bonding pair. However, this angle is also greater than 90°, which would be predicted for largely *p* orbital bonding between Sb and its ligands. We address this point later in the article.

Each Na ion is surrounded by six Te atoms at distances ranging between 3.216 and 3.453 Å which form distorted trigonal antiprisms. The differences among these cation sites become apparent when the $[SbTe_3]^{-3}$ anions are considered to be the coordinating anions, see Figs. 2b–2d. For Na1, three close Te contacts arise from a single $[SbTe_3]^{-3}$ pyramid, which also provides a relatively short Na–Sb distance of 3.679 Å. Three and six $[SbTe_3]^{-3}$ groups, respectively, form the coordination polyhedra for Na2 and Na3. These two environments are related to possible Na coordinations found in $NaSbTe_2$ (9). This compound adopts the rocksalt structure with Na and Sb randomly arranged on one of the sites in NaCl. In the rocksalt geometry, (Na, Sb) sites interact with each other either by sharing edges or vertices of coordinating Te octahedra. The first and second nearest neighbor environment for Na2 in Na_3SbTe_3 (six Te atoms and three Sb atoms via edge-sharing) would occur for ca. 5% of the Na atoms in $NaSbTe_2$, while the analogous surroundings for Na3 (six Te atoms and six Sb atoms via vertex-sharing) would occur for only 2% of the Na atoms. Finally, the Na1 coordination geometry is not possible in a rocksalt framework.

The arrangement of the cations in the structure of Na_3SbTe_3 is related to the Li_3Bi structure type (15, 24). In Li_3Bi, Bi atoms form a cubic closest packing (ccp) with all of the octahedral and tetrahedral holes occupied by lithium atoms. If we assume all atoms in "Li_3Bi" to be identical, then the entire Li_3Bi structure is simply a body-centered cubic packing (bcc) of atoms. In Na_3SbTe_3, at first sight, the Sb atoms form the ccp and the Na atoms occupy all octahedral (Na3) and tetrahedral (Na1 and Na2) interstices. To understand the arrangement of Te atoms in the Na_3SbTe_3 structure, we now adopt the viewpoint of a bcc packing of Na and Sb atoms. In bcc packing there are three rectangular bipyramidal ("octahedral") holes per atom. In the Na_3SbTe_3 structure, one-fourth of

these are occupied by Te atoms in an ordered way such that each Sb atom is surrounded by three Te atoms. In addition, displacements of both the Na and Te atoms from ideal sites give a coordination at each Te position by six Na atoms and one Sb atom.

Interestingly, the structure of K_3AsS_4 (25) can also be described in the same way as Na_3SbTe_3. In K_3AsS_4, however, one-third of the rectangular bipyramidal holes in the cation packing arrangements are filled, rather than one-fourth as in Na_3SbTe_3.

What factors control the observed arrangement of $[SbTe_3]^{-3}$ groups in Na_3SbTe_3? To answer this question requires enumeration of all possibilities followed by the evaluation of the structural energy according to some prescription, whether it involves classical or quantum mechanical methods (26, 27). Structure enumeration involves setting some constraints under which the various possibilities may arise. In the case of alternatives to Na_3SbTe_3, we have adopted the following criteria: (i) the observed unit cell metrics were chosen in order to maintain four formula units per unit cell; (ii) the Na and Sb positions are ideally set to the Li and Bi positions in the Li_3Bi structure (space group $Fm\bar{3}m$); and (iii) the three Te atoms of each $[SbTe_3]^{-3}$ unit occupy confacial sites of a regular octahedron surrounding each Sb atom. Different patterns emerge because there are four Sb atoms per unit cell, each with eight orientations of the three Te ligands (there are eight faces of an octahedron). With this treatment, we are treating each $[SbTe_3]^{-3}$ fragment essentially as a molecular dipole. If we would allow rotations of these pyramids about their threefold axes at this point, an infinite number of orientations exist.

Under this set of constraints, we generate $8^4 = 4096$ possibilities (8 orientations, 4 sites), but the actual number will be much less because any one structure is equivalent to others obtained by some symmetry operation of the space group $Fm\bar{3}m$ of the Li_3Bi parent structure. In other words, the group $Fm\bar{3}m$ divides the set of 4096 structures into equivalence classes called orbits, and to enumerate the distinct structures, we must count these orbits. The counting procedure involves Burnside's lemma (28), which states that the number, Ω, of orbits is given by

$$\Omega = |G|^{-1} \sum_{g \in G} \Phi(g), \qquad [1]$$

where $|G|$ is the order of the group G, g is a symmetry operation in G, and $\Phi(g) = |\{s \in S : gs = s\}|$ is the number of operations s that are fixed by the operation g of G.

In this problem, G is the space group $Fm\bar{3}m$ and S is the set of 4096 arrangements of Te atoms. To apply Burnside's lemma, we must replace the infinite group $Fm\bar{3}m$ with a finite group of permutations of the set S. Such a group is the quotient group, $Fm\bar{3}m/P1$, since every translation of $Fm\bar{3}m$ corresponds to the identity permutation on S. This group has order 192. Since the Te atoms are linked to each of the four Sb atoms, which themselves form a tetrahedron within the unit cell, the operations of this quotient group may be derived as the product of the point group $\bar{4}3m$ (of the point $(\frac{1}{4}, \frac{1}{4}, \frac{1}{4})$ in the $Fm\bar{3}m$ cell; $\{1, 3_{111}, \bar{4}_{100}, 2_{100}, m_{110}\}$) and the set of rotations and reflections $\{1, 2_{100}, 2_{010}, 2_{001}, \bar{1}, m_{100}, m_{010}, m_{001}\}$. Table 4 summarizes the application of Burnside's lemma to this problem by listing the value of $\Phi(g)$ for every $g \in Fm\bar{3}m/P1$. The total number of orbits divided by the 192 symmetry operations in the quotient group gives 42 structural alternatives.

TABLE 4
Application of Burnside's Lemma to Evaluate Possible A_3PnX_3 Structures

g	Number of g	$\Phi(g)$
1	1	4096
3_{111}	8	16
2_{100}	3	64
$\bar{4}_{100}$	6	8
m_{110}	6	128
$\bar{1}$	1	0
$3_{111} \cdot \bar{1}$	8	0
$2_{100} \cdot \bar{1}$	3	64
$\bar{4}_{100} \cdot \bar{1}$	6	8
$m_{110} \cdot \bar{1}$	6	0
m_{100}	3	0
$3_{111} \cdot m_{100}$	24	0
$\bar{4}_{100} \cdot m_{100}$	6	8
$4_{100} \cdot m_{010}$	12	8
$2_{100} \cdot m_{100}$	3	64
$2_{100} \cdot m_{010}$	6	64
$m_{110} \cdot m_{100}$	12	0
$m_{110} \cdot m_{001}$	6	0
2_{100}	3	0
$3_{111} \cdot 2_{100}$	24	32
$\bar{4}_{100} \cdot 2_{100}$	6	8
$\bar{4}_{100} \cdot 2_{010}$	12	8
$2_{100} \cdot 2_{100}$	3	64
$2_{100} \cdot 2_{010}$	6	64
$m_{110} \cdot 2_{100}$	12	0
$m_{110} \cdot 2_{001}$	6	64
Total	192	8064

Next, we need to assess the energetics for each of the 42 inequivalent structures. The simplest ideas would immediately conclude that covalent forces control bonding within $[SbTe_3]^{-3}$ groups, and these interact with each other and the Na ions via ionic forces. Since each $[SbTe_3]^{-3}$ fragment may be treated as a molecular dipole anion, we have utilized lattice energy calculations that take into account Madelung, Born–Mayer repulsion, and van der Waals attraction terms (29). Details of these calcu-

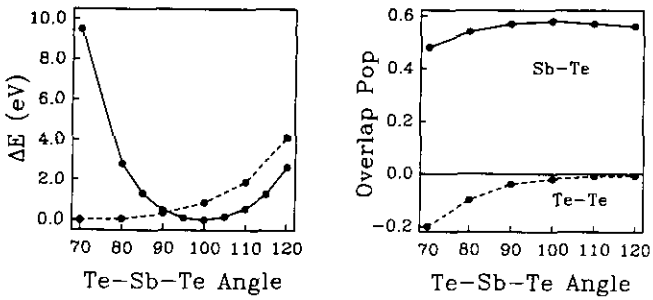

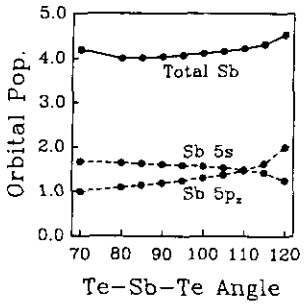

FIG. 3. Variations in total energies, overlap populations, and orbital populations in $[SbTe_3]^{-3}$ groups as a function of the Te–Sb–Te angle. In the ΔE plot: (solid) all overlaps; (dashed) Sb–Te overlaps only.

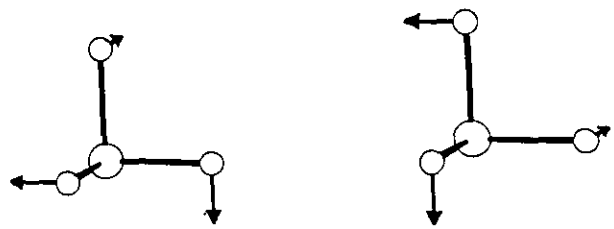

SCHEME 1

lations are outlined in the Appendix. Under the set of constraints listed previously, the minimum energy structure (highest lattice energy, U_{LAT}) for Na_3SbTe_3 has all $[SbTe_3]^{-3}$ fragments identically oriented. This arrangement also has the highest (most negative) Madelung term. The resulting structure is rhombohedral, $R3m$, $Z = 1$, and represents a structure type that is related to Tl_3SbS_3 (30) and Tl_3AsS_3 (31). However, the $[PnS_3]^{-3}$ ions adopt bcc rather than ccp packing ($\alpha_R \approx 105°$ for both compounds). This arrangement of trigonal pyramidal anions also occurs in alkali metal chlorates, bromates, and iodates (32), and has recently been reported for the series $CsGeX_3$ (X = Cl, Br, I) (33), which is related to the cubic perovskite structure. Since the Te–Sb–Te angle in each $[SbTe_3]^{-3}$ group is 90° for these model calculations, what happens as we adjust the Te atom positions away from this angle constraint but maintain the threefold axis of symmetry?

The results of extended Hückel calculations (34) on isolated $[SbTe_3]^{-3}$ units are shown in Fig. 3, in which various parameters are plotted as a function of the Te–Sb–Te angle. The total energies of two scenarios are depicted in Fig. 3a: (i) all orbital overlaps; (ii) only Sb–Te orbital overlaps are included. The results clearly show that Te–Te interactions crucially affect the observed geometry of the $[SbTe_3]^{-3}$ group; the minimum energy is found when the Te–Sb–Te angle is slightly above 99° in case (i), but drops to near 70° in case (ii). To understand this conclusion in terms of orbital interactions, we have also evaluated trends in Sb–Te overlap population as well as Sb 5s and 5p_z orbital occupations with this angle. Both provide clues to the electronic influence on the local geometry. After examining the nature of the HOMO we find not only nonbonded repulsions between Te atoms, but also subtle effects on the Sb–Te interactions. Near the trigonal planar geometry, the sp hybridization at Te along the Sb–Te bond is directed towards Sb in the HOMO, but significant π^* Sb–Te overlap that mixes into the HOMO for angles slightly away from 120° drives pyramidalization via a second order Jahn–Teller effect (35). As the angle narrows and Te–Te distances decrease, Te–Te orbital interactions force the sp hybridization away from Sb. Thus, we find an angle of 100° due not only to Te–Te repulsions, but also to subtle changes in Sb–Te σ orbital overlaps as a function of angle.

Within our set of 42 Na_3SbTe_3 possibilities, we can adjust the Te atom positions about each Sb atom to give a Te–Sb–Te angle close to 100° by taking a linear combination of the two orthogonal rotations depicted in Scheme 1. Each independent rotation causes the Te atoms to shift away from an octahedral and toward a tetrahedral hole in the bcc packing of cations. Generally, we found that the most energetically favorable shift of each trigonal pyramid for a particular arrangement was *one* of the two rotations in Scheme 1. With this additional degree of freedom, the structure giving the greatest lattice energy turned out to

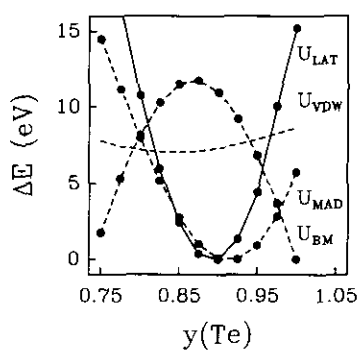

FIG. 4. Variations in lattice energy (U_{LAT}, solid), Madelung energy (U_{MAD}, dashed), Born–Mayer repulsion (U_{BM}, dashed), and van der Waals energy (U_{VDW}, dashed) in the $P2_13$ structure of Na_3SbTe_3 as a function of y(Te). The observed y(Te) is nearly 0.88.

TABLE 5
Space Group Symmetries for the 42 Different Arrangements for Na_3SbTe_3

No.	Space group	$-U_{LAT}$ (eV)	Z	No.	Space group	$-U_{LAT}$ (eV)	Z	No.	Space group	$-U_{LAT}$ (eV)	Z
1	$P2_13$	0.00	4	15	$C2$	5.06	2	29	Cm	6.37	2
2	$Pca2_1$	2.27	4	16	$P1$	5.10	4	30	Cm	6.41	2
3	$P2_1/c$	2.41	4	17	$P1$	5.12	4	31	$P1$	6.58	4
4	$Pna2_1$	2.71	4	18	$P2/c$	5.13	4	32	Cm	6.72	2
5	$P1$	2.75	4	19	$P1$	5.14	4	33	$P1$	6.75	4
6	$P1$	3.84	4	20	Cm	5.16	2	34	Cm	6.76	2
7	$R3$	3.87	4	21	$P1$	5.30	4	35	Cm	7.00	2
8	$P1$	3.89	4	22	$Pmn2_1$	5.35	4	36	$R3m$	7.00	1
9	$P1$	4.04	4	23	$P1$	5.43	4	37	Cm	7.34	2
10	$P1$	4.07	4	24	Cm	5.52	4	38	$R3m$	7.67	4
11	$Pmn2_1$	4.54	2	25	$P1$	5.65	4	39	$P2_1/m$	7.89	2
12	$P1$	4.92	4	26	$P\bar{4}2_1m$	5.74	4	40	$P\bar{4}3m$	8.17	4
13	$Pcc2$	4.93	4	27	$P2_1/n$	5.86	4	41	$R3m$	8.71	4
14	Cc	5.05	2	28	Cm	6.15	2	42	$P4_2nm$	8.89	4

Note. The different structures are listed according to decreasing lattice energy; the most stable structure is first. Z = Number of formula units.

be the observed structure of Na_3SbTe_3, which was approximately 2.3 eV (220 kJ/mole) more stable than the second best case. Not only does this structure provide the highest Madelung contribution to the lattice energy, but also the lowest Born–Mayer repulsion term. Table 5 summarizes the results of these calculations by listing the space groups for the 42 possible structrues, their relative energies, and the number of formula units per primitive cell.

Within the space group $P2_13$, we have also searched for the greatest lattice energy as a function of Te atom positions. Crystallographically, Te occupies a general position, but $x(\text{Te}) \approx 0.25$ and $z(\text{Te}) \approx 0$. Therefore, Fig. 4 shows a plot of the lattice energy and various contributions to the lattice energy vs y(Te). The lattice energy maximum occurs around $y(\text{Te}) = 0.88$, in excellent agreement with observation, and results as an optimization in both the Madelung term as well as the Born–Mayer repulsion term.

Thus, the structure of Na_3SbTe_3 and its analogs are controlled by both covalent as well as ionic forces. Covalent interactions within each $[SbTe_3]^{-3}$ anion greatly influence its observed local geometry, while long-range Coulomb and short-range Born–Mayer repulsions dictate the arrangement of these anions in the cation matrix.

APPENDIX

Extended Hückel calculations. Calculations on the trigonal pyramidal $[SbTe_3]^{-3}$ fragments were carried out for d(Sb–Te) = 2.787 Å, both as isolated anions as well as packed in the $P2_13$ space group. Atomic orbital parameters for Sb and Te valence orbitals are listed in Table 6.

Lattice energy calculations. The lattice energy U_{LAT} of a crystal can be approximately expressed as

TABLE 6
Atomic Parameters for Lattice Energy and Extended Hückel calculations on Na_3SbTe_3

	Na	Sb	Te
q_i	+1	+3	−2
$r^{(0)}$ (Å)	0.93	0.93	1.93
α (Å^3)	0.181	1.25	9.22
ε (eV)	35.50	33.20	5.90
p	8.00	2.00	4.00
ζ_{5s}	—	2.32	2.51
H_{ss} (eV)	—	−18.80	−20.80
ζ_{5p}	—	2.00	2.16
H_{pp} (eV)	—	−11.70	−14.80

Note. See the Appendix for brief descriptions of these variables.

$$U_{LAT} \approx U_{MAD} + U_{BM} + U_{VDW}, \quad [2]$$

where U_{MAD} is the Madelung energy (Coulomb interactions), U_{BM} is the Born–Mayer repulsion energy, and U_{VDW} is the van der Waals energy. We have not included a zero-point energy term (29). Each term is expressed as follows:

$$U_{MAD} = 14.40 \sum_{ij}{}' q_i q_j / r_{ij}, \quad [3]$$

$$U_{BM} = b \sum_{ij}{}' (1 + q_i/r_i^{(0)} + q_j/r_j^{(0)}) \exp(-r_{ij}/\rho), \quad [4]$$

$$U_{VDW} = \sum_{ij}{}' c_{ij}/r_{ij}^6 + d_{ij}/r_{ij}^8, \quad [5]$$

where

$$c_{ij} = 1.5\,\alpha_i\alpha_j[\varepsilon_i\varepsilon_j/(\varepsilon_i + \varepsilon_j)]\ (\text{eV}\cdot\text{Å}^6) \quad [6]$$

$$d_{ij} = 0.156\,c_{ij}[(\alpha_i\varepsilon_i/p_i) + (\alpha_j\varepsilon_j/p_j)]\ (\text{eV}\cdot\text{Å}^8). \quad [7]$$

Table 6 lists the various atomic parameters utilized in these equations. In Eqs. [3]–[5], the summations are carried out over all pairs of atoms $\{ij\}$ except when $i = j$. The $r^{(0)}$ values are the so-called "basic radii" for ions as used by Bevan and Morris (36). Here, α represents polarizabilities, which are evaluated from the gas phase refraction indices for cations after Pauling (37) and estimated from experimental refraction data on ionic crystals for the anions (38). The characteristic energies ε and the effective number of outer electrons p follow Mayer's recommendations (39). Also, $\rho = 0.345$ Å. The scaling constant b in Eq. [4] was evaluated by using the equilibrium condition, i.e.,

$$\left(\frac{dU_{\text{LAT}}}{dr}\right)\Bigg|_{r=r_0} = 0, \quad [8]$$

for the observed Na_3SbTe_3 structured and $r_0 \equiv$ minimum cation–anion distance in the compound (2.787 Å). Then, $b = 0.71$ eV · Å. The Madelung energy, U_{MAD}, is evaluated using the Ewald method (40).

ACKNOWLEDGMENTS

We wish to thank Professor R. A. Jacobson for the use of a Siemens P4 single crystal diffractomenter, and J. E. Ostenson for magnetic susceptibility measurements. This project was supported both by the Chemical Sciences Division, Office of Basic Energy Sciences, U.S. Department of Energy, under Contract W-7405-Eng-82 and the donors of the Petroleum Research Fund, administered by the American Chemical Society.

REFERENCES

1. H. Schäfer and B. Eisenmann, *Rev. Inorg. Chem.* **3,** 29 (1981).
2. R. Zagler, "Darstellung und Strukturchemie von Chalkogenido-Polyanionen und Chalkogenidoindaten, -germaniten, -stannaten, -arsenaten, antimonaten bzw. -telluraten mit komplexierten und nicht komplexierten Kationen," Thesis, Darmstadt, 1988.
3. B. Eisenmann and R. Zagler, *Z. Kristallogr.* **197,** 255 (1991).
4. B. Eisenmann and R. Zagler, *Z. Kristallogr.* **197,** 257 (1991).
5. B. Eisenmann, R. Jäger, and R. Zagler, *Z. Kristallogr.* **197,** 259 (1991).
6. B. Eisenmann and R. Zagler, *Z. Kristallogr.* **197,** 261 (1991).
7. J.-S. Jung, B. Wu, E. D. Stevens, and C. J. O'Connor, *J. Solid State Chem.* **94,** 362 (1991).
8. M. Evain, F. Boucher, R. Brec, J. Rouxel, J.-S. Jung, and C. J. O'Connor, *Eur. J. Solid State Inorg. Chem.* **29,** 1055 (1992).
9. B. Eisenmann and H. Schäfer, *Z. Anorg. Allg. Chem.* **456,** 87 (1979).
10. A. F. Trippel', V. B. Lazarev and S. I. Berul', *Zh. Neorg. Khim.* **23,** 707 (1978); *Russ. J. Inorg. Chem.*
11. P. M. Keane, Y.-J. Lu and J. A. Ibers, *Acc. Chem. Res.* **24,** 223 (1991).
12. P. Böttcher, *Angew. Chem.* **100,** 781 (1988); *Angew. Chem. Int. Ed. Engl.* **27,** 759 (1988).
13. E. Zintl and G. Brauer, *Z. Phys. Chem. B* **20,** 245 (1933); E. Zintl, *Angew. Chem.* **52,** 1 (1939); H. G. von Schnering, *Nova Acta Leopold,* **59,** 264 (1985); H. Schäfer, *Annu. Rev. Mater. Sci.* **15,** 1 (1985).
14. L. Pauling, "The Nature of the Chemical Bond," 3rd ed., p. 93. Cornell Univ. Press, Ithaca, NY, 1960.
15. V. H. Sommer and R. Hoppe, *Z. Anorg. Allg. Chem.* **430,** 199 (1977).
16. V. B. Lazarev, L. M. Kavba, N. A. Moshchalkova, and A. V. Salov, *Zh. Neorg. Khim.* **23,** 2502 (1978); *Russ. J. Inorg. Chem.* **23,** 1381 (1978).
17. K.-J. Range, M. Zabel, F. von Krziwanek, R. Marx, and B. Panzer, *Angew. Chem.* **94,** 717 (1982); *Angew. Chem. Int. Ed. Engl.* **21,** 706 (1982).
18. SHELXTL-PLUS, Version 4.0, Siemens Industrial Automation, Inc., Madison, WI.
19. G. M. Sheldrick, in preparation.
20. "International Table for X-Ray Crystallography," Vol. C, Kynoch, Birmingham, England, 1992.
21. J. Galy, G. Meunier, S. Andersson, and A. Åström *J. Solid State Chem.* **9,** 92 (1975).
22. B. G. Hyde and S. Andersson, "Inorganic Crystal Structures," Chap. X. Wiley, New York, 1989.
23. J. Trotter and T. Zobel, *Z. Kristallogr.* **123,** 67 (1966); S. Pohl and W. Saak, *Z. Kristallogr.* **169,** 177 (1984).
24. P. Villars and L. D. Calvert, "Parson's Handbook of Crystallographic Data for Intermetallic Phases,," Vol. 1. Am. Soc. Metals, Metals Park, OH 1985.
25. P. M. Palazzi, S. Jaulmes, and P. Laruelle, *Acta Crystallogr Sect. B* **30,** 2378 (1974).
26. J. K. Burdett, T. J. McLarnan, and P. Haaland, *J. Chem. Phys.* **75,** 5774 (1981).
27. J. K. Burdett and T. J. McLarnan, *Inorg. Chem.* **21,** 1119 (1982).
28. W. S. Burnside, "Theory of Groups of Finite Order," 2nd ed. Dover Publications, New York, 1955, C. L. Liu, "Introduction to Combinatorial Mathematics." McGraw–Hill, New York, 1968, D. H. Rouvray, *Chem. Rev.* **3,** 355 (1974); T. J. McLarnan and P. B. Moore, *in* "Structure and Bonding in Solids" (M. O'Keeffe and A. Navrotsky, Eds.), Vol. I. Academic Press, New York, 1981.
29. F. Seitz, "The Modern Theory of Solids," Chap. II. Dover Publications, New York, 1987; N.N. Greenwood, "Ionic Crystals, Lattice Defects, and Nonstoichiometry." Butterworths, London, 1968.
30. N. Rey, J. C. Jumas, J. Olivier-Fourcade, and E. Philippot, *Acta Crystallogr. Sect. C* **40,** 1655 (1984).
31. M. Gostojic, *Z. Kristallogr.* **151,** 249 (1980).
32. R. W. K. Wyckoff, "Crystal Structures," 2nd ed., Vol. 1. Wiley, New York, 1960.
33. G. Thiele, H. W. Rotter, and K. D. Schmidt, *Z. Anorg. Allg. Chem.* **545,** 148 (1987).
34. R. Hoffmann and W. N. Lipscomb *J. Chem. Phys.* **36,** 2179, 3489 (1962); R. Hoffmann, *J. Chem. Phys.* **39,** 1397 (1963); J. H. Ammeter, H.-B. Bürgi, J. C. Thibeault, and R. Hoffmann, *J. Am. Chem. Soc.* **100,** 3686 (1978).
35. J. K. Burdett, "Molecular Shapes," Wiley–Interscience, New York, 1980.
36. S. C. Bevan and D. F. C. Morris, *J. Chem. Soc.* 516 (1960).
37. L. Pauling, *Proc. R. Soc. London Ser. A* **114,** 191 (1927).
38. S. S. Jaswal and T. P. Sharma, *J. Phys. Chem. Solids* **34,** 509 (1973); J. R. Tessman, A. H. Kahn, and W. Shockley, *Phys. Rev.* **92,** 890 (1953).
39. J. E. Mayer, *J. Chem. Phys.* **1,** 270 (1933).
40. J. M. Ziman, "Principles of the Theory of Solids," p. 39. Cambridge Univ. Press, London, 1964.